

# Channel Estimation for RIS-Assisted mmWave Systems via Diffusion Models

Yang Wang, Yin Xu, Cixiao Zhang, Zhiyong Chen, Mingzeng Dai, Haiming Wang, Bingchao Liu,  
Dazhi He, and Meixia Tao, *Fellow, IEEE*,

**Abstract**—Reconfigurable intelligent surface (RIS) has been recognized as a promising technology for next-generation wireless communications. However, the performance of RIS-assisted systems critically depends on accurate channel state information (CSI). To address this challenge, this letter proposes a novel channel estimation method for RIS-aided millimeter-wave (mmWave) systems based on diffusion models (DMs). Specifically, the forward diffusion process of the original signal is formulated to model the received signal as a noisy observation within the framework of DMs. Subsequently, the channel estimation task is formulated as the reverse diffusion process, and a sampling algorithm based on denoising diffusion implicit models (DDIMs) is developed to enable effective inference. Furthermore, a lightweight neural network, termed BRCNet, is introduced to replace the conventional U-Net, significantly reducing the number of parameters and computational complexity. Extensive experiments conducted under various scenarios demonstrate that the proposed method consistently outperforms existing baselines.

**Index Terms**—Diffusion models, channel estimation, reconfigurable intelligent surface.

## I. INTRODUCTION

MILLIMETER-WAVE (mmWave) communication is a key technology for the sixth generation (6G) communication systems to fully exploit the available spectrum [1]. Nevertheless, the coverage range of mmWave signals is limited due to their rapid attenuation, which makes them susceptible to blockage. To overcome this limitation, reconfigurable intelligent surfaces (RISs) [2] have been introduced to extend communication coverage and improve transmission rates. However, the effectiveness of the RIS depends on accurate channel state information (CSI). In general, a RIS consists of passive elements without signal processing capabilities, which poses a significant challenge for channel estimation in RIS-assisted systems.

Conventional methods (e.g., linear minimum mean square error, LMMSE) and compressed sensing (CS)-based methods (e.g., the double-structured orthogonal matching pursuit, DS-OMP [3]) struggle to achieve accurate channel estimation

under low signal-to-noise ratio (SNR) conditions. With the rapid development of artificial intelligence (AI), deep learning (DL)-based methods have been increasingly applied in RIS-assisted systems. For instance, a convolutional neural network (CNN)-based method is proposed in [4], where a deep residual network (DRN) is used to denoise the results obtained from the least squares (LS) estimator. Furthermore, a global attention residual network (GARN) is introduced to fuse multi-channel information and improve the accuracy of channel estimation [5]. However, these direct-mapping DL methods require network retraining for different SNRs, limiting their generalizability and practicality.

Recently, diffusion models (DMs) [6] have emerged as powerful generative AI techniques capable of modeling complex data distributions. To leverage their strengths, various studies have explored the application of DMs in wireless communications. Specifically, channel denoising diffusion models (CD-DMs) are proposed in [7] as a separate module following the channel equalizer. In [8], DMs are integrated with low-density parity-check (LDPC) decoding to enhance error correction. Moreover, DMs are applied to high-dimensional channel estimation in [9]. Among these applications, channel estimation has garnered particular attention due to its critical role in communication systems. In [10], guided DMs are employed for channel estimation, yet the U-Net architecture introduces significant memory and computational overhead. To address this issue, a CNN-based network that achieves lower overhead is proposed in [11]. Nevertheless, this simplified architecture suffers from performance degradation in more complex propagation environments. Therefore, achieving accurate and efficient channel estimation in RIS-assisted systems remains a challenging problem that requires further investigation.

In this letter, we propose a novel channel estimation method for RIS-assisted mmWave systems based on DMs. The key contributions are summarized as follows

- We formulate the channel estimation problem in RIS-assisted systems as the reverse denoising process of denoising diffusion implicit models (DDIMs). This approach inherently adapts to dynamic noise conditions through a step-matching mechanism.
- We first propose a U-Net-based channel estimation scheme and subsequently develop a parameter-efficient network architecture, referred to as BRCNet, to reduce model complexity and computational overhead.
- Extensive simulations demonstrate that the proposed method outperforms the baselines across various scenarios, while the BRCNet achieves performance comparable to U-Net using only 9.34% of its parameters.

This work was supported in part by the Shanghai Municipal Education Commission (No. 2024A1YB002) and the National Natural Science Foundation of China Program (62422111).

Yang Wang, Yin Xu (*Senior Member, IEEE*), Cixiao Zhang, Zhiyong Chen (*Senior Member, IEEE*), Dazhi He (*Senior Member, IEEE*), and Meixia Tao (*Fellow, IEEE*) are with the Cooperative Medianet Innovation Center, Shanghai Jiao Tong University, Shanghai 200240, China (e-mail: {vy\_eddie, xuyin, cixiaozhang, zhiyongchen, hedazhi, mxtao}@sjtu.edu.cn).

Mingzeng Dai is with the Lenovo Group, Lenovo Research, Shanghai 201203, China (e-mail: daimz4@lenovo.com). Haiming Wang and Bingchao Liu are with the Lenovo Group, Lenovo Research, Beijing 2100094, China (e-mail: {wanghm14, liubc2}@lenovo.com).

The corresponding author is Yin Xu.

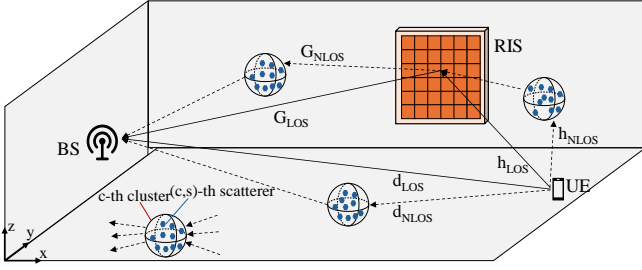


Fig. 1. RIS-assisted mmWave communication systems.

## II. SYSTEM MODEL

### A. Channel Model

As illustrated in Fig. 1, we consider the uplink channel estimation for RIS-assisted mmWave systems. Both the base station (BS) and RIS are equipped with uniform planar arrays (UPAs) with half-wavelength element spacing, while the user equipment (UE) has a single antenna. The BS has  $M = M_h \times M_v$  antennas, and the RIS consists of  $N = N_h \times N_v$  passive elements. The UE-BS, UE-RIS, and RIS-BS channels are denoted as  $\mathbf{d} \in \mathbb{C}^{M \times 1}$ ,  $\mathbf{h} \in \mathbb{C}^{N \times 1}$ , and  $\mathbf{G} \in \mathbb{C}^{M \times N}$ , respectively. Following [12] and [13], a clustered statistical channel model is adopted. The RIS-BS channel consists of line-of-sight (LOS) and non-line-of-sight (NLOS) components, i.e.,  $\mathbf{G} = \mathbf{G}_{\text{LOS}} + \mathbf{G}_{\text{NLOS}}$ . These two components are represented as

$$\mathbf{G}_{\text{LOS}} = \sqrt{G_e(\varphi_{\text{LOS}}^{G_t})} L_{\text{RIS-BS}} \mathbf{a}_{\text{BS}}(\phi_{\text{LOS}}^{G_r}, \varphi_{\text{LOS}}^{G_r}) \times \mathbf{a}_{\text{RIS}}^T(\phi_{\text{LOS}}^{G_t}, \varphi_{\text{LOS}}^{G_t}), \quad (1)$$

$$\mathbf{G}_{\text{NLOS}} = \gamma^G \sum_{c=1}^{C^G} \sum_{s=1}^{S_c^G} \beta_{c,s}^G \sqrt{G_e(\varphi_{c,s}^{G_t})} L_{c,s}^{G_t} \mathbf{a}_{\text{BS}}(\phi_{c,s}^{G_r}, \varphi_{c,s}^{G_r}) \times \mathbf{a}_{\text{RIS}}^T(\phi_{c,s}^{G_t}, \varphi_{c,s}^{G_t}), \quad (2)$$

where  $C^G$  and  $S_c^G$  denote the number of clusters and the number of scatterers in the  $c$ -th cluster, respectively. The normalization factor is defined as  $\gamma^G = \sqrt{\frac{1}{\sum_{c=1}^{C^G} S_c^G} \cdot \beta_{c,s}^G} \sim \mathcal{CN}(0, 1)$  denotes the path gain of the  $(c, s)$ -th scatterer, which follows a circularly symmetric complex Gaussian (CSCG) distribution. The element radiation pattern of the RIS corresponding to the  $(c, s)$ -th scatterer is defined as  $G_e(\varphi_{c,s}^{G_t}) = 2(2\zeta + 1) \cos^2 \zeta(\varphi_{c,s}^{G_t})$  [14]. The path loss  $L_{c,s}^{G_t}$  is defined as

$$L_{c,s}^{G_t} = -20 \log_{10} \left( \frac{4\pi}{\lambda} \right) - 10n \left( 1 + b \left( \frac{f_c - f_0}{f_0} \right) \right) \log_{10}(d_{c,s}) - X_{\sigma_x}, \quad (3)$$

where  $\lambda$  is the carrier wavelength,  $n$  is the path loss exponent,  $b$  is a system parameter,  $f_0$  is the reference frequency,  $f_c$  is the carrier frequency,  $d_{c,s}$  is the propagation distance of the  $(c, s)$ -th scatterer, and  $X_{\sigma_x} \sim \mathcal{CN}(0, \sigma_x^2)$  is the shadow factor.

$\mathbf{a}_{\text{BS}}(\phi_{c,s}^{G_r}, \varphi_{c,s}^{G_r})$  and  $\mathbf{a}_{\text{RIS}}(\phi_{c,s}^{G_t}, \varphi_{c,s}^{G_t})$  denote the steering vectors of the BS and the RIS, respectively. Here,  $\phi_{c,s}^{G_r}$  and  $\varphi_{c,s}^{G_r}$  represent the azimuth and elevation angles of arrival (AOA), respectively, while  $\phi_{c,s}^{G_t}$  and  $\varphi_{c,s}^{G_t}$  denote the corresponding angles of departure (AOD).  $\phi_{c,s}^{G_t}$  follows a Laplacian distribution  $\mathcal{L}(\phi_{c,s}^{G_t}, \sigma_\phi)$ , where  $\phi_{c,s}^{G_t}$  follows a uniform distribution  $\mathcal{U}[-\pi/2, \pi/2]$  and  $\sigma_\phi$  represents the angular spread. Similarly,  $\varphi_{c,s}^{G_t}$  follows  $\mathcal{L}(\varphi_{c,s}^{G_t}, \sigma_\varphi)$  with  $\varphi_{c,s}^{G_t} \sim \mathcal{U}[-\pi/4, \pi/4]$ . The UPA steering vectors can be written as

$$\mathbf{a}(\phi, \varphi) = [1, \dots, e^{j2\pi d(x \sin \varphi + y \sin \phi \cos \varphi)/\lambda}, \dots, e^{j2\pi d((N_h-1) \sin \varphi + (N_v-1) \sin \phi \cos \varphi)/\lambda}]^T, \quad (4)$$

where  $0 \leq x \leq N_h - 1$  and  $0 \leq y \leq N_v - 1$ , and  $d$  denotes the element spacing. Similarly, the UE-RIS channel  $\mathbf{h}$  and the UE-BS channel  $\mathbf{d}$  share the same structural form as  $\mathbf{G}$ .

### B. Signal Model

The received signal  $\mathbf{y}_k \in \mathbb{C}^{M \times 1}$  in the  $k$ -th time slot can be expressed as

$$\mathbf{y}_k = (\mathbf{d} + \mathbf{G} \text{diag}(\boldsymbol{\omega}_k) \mathbf{h}) x_k + \mathbf{n}, \quad (5)$$

where  $\mathbf{n} \sim \mathcal{CN}(0, 2\sigma^2 \mathbf{I})$  denotes the additive white Gaussian noise (AWGN),  $x_k$  is the pilot symbol, and  $\text{diag}(\cdot)$  denotes the diagonal operator. The phase shift vector is given by  $\boldsymbol{\omega}_k = [\beta_1 e^{j\theta_1}, \beta_2 e^{j\theta_2}, \dots, \beta_N e^{j\theta_N}]^T$ , where  $\beta_n \in [0, 1]$  and  $\theta_n \in [-\pi, \pi)$  represent the amplitude and the phase shift of the  $n$ -th element, respectively. The channel of the reflecting link UE-RIS-BS can be rewritten as  $\mathbf{G} \text{diag}(\boldsymbol{\omega}_k) \mathbf{h} = \mathbf{G} \text{diag}(\mathbf{h}) \boldsymbol{\omega}_k$ . We define the cascaded channel as  $\mathbf{H}_c = \mathbf{G} \text{diag}(\mathbf{h})$  and the augmented phase shift vector  $\mathbf{p}_k = [1, \boldsymbol{\omega}_k^T]^T \in \mathbb{C}^{(N+1) \times 1}$ . Based on (5), the received signal can be expressed as

$$\mathbf{y}_k = \mathbf{H} \mathbf{p}_k x_k + \mathbf{n}, \quad (6)$$

where  $\mathbf{H} = [\mathbf{d}, \mathbf{H}_c] \in \mathbb{C}^{M \times (N+1)}$ . Without loss of generality, the pilot symbol is set to  $x_k = 1$  [5], [10]. After  $K$  time slots, the received signal  $\mathbf{Y} \in \mathbb{C}^{M \times K}$  is given by

$$\mathbf{Y} = \mathbf{H} \mathbf{P} + \mathbf{N}. \quad (7)$$

The RIS reflecting matrix is set as the columns of the discrete Fourier transform (DFT) matrix [15]. The objective of channel estimation is to recover the unknown channel  $\mathbf{H}$  from the received signal  $\mathbf{Y}$ . By vectorizing (7), we obtain

$$\text{vec}(\mathbf{Y}) = (\mathbf{I}_K \otimes \mathbf{H}) \cdot \text{vec}(\mathbf{P}) + \text{vec}(\mathbf{N}), \quad (8)$$

where  $\text{vec}(\cdot)$  denotes vectorization and  $\otimes$  denotes the Kronecker product. Given the noise power  $\sigma^2$ , (8) is normalized and converted into an equivalent real-valued form as

$$\mathbf{y} = \frac{1}{\sqrt{1 + \sigma^2}} \mathbf{A} \mathbf{p} + \frac{\sigma}{\sqrt{1 + \sigma^2}} \mathbf{n}, \quad (9)$$

where  $\mathbf{y} \in \mathbb{R}^{2MK \times 1}$ ,  $\mathbf{A} \in \mathbb{R}^{2MK \times 2(N+1)K}$ ,  $\mathbf{p} \in \mathbb{R}^{2(N+1)K \times 1}$ , and  $\mathbf{n} \in \mathbb{R}^{2MK \times 1}$  with entries distributed as  $n_i \sim \mathcal{N}(0, 1)$ .

### III. PROPOSED METHOD

This section details the proposed method. First, a forward diffusion process for the received signal is formulated to define the training algorithm. Then, a sampling algorithm based on the DDIM is developed. Furthermore, a lightweight neural network architecture, termed BRCNet, is designed to reduce the model complexity and computational overhead.

#### A. Training Algorithm of the Proposed Method

The original signal  $\mathbf{x}_0$  is defined as  $\mathbf{x}_0 = \mathbf{A}\mathbf{p}$ . By progressively adding noise to  $\mathbf{x}_0$ , the signal at step  $t \in \{1, 2, \dots, T\}$  is obtained as follows

$$\mathbf{x}_t = \sqrt{1 - \beta_t} \mathbf{x}_{t-1} + \beta_t \boldsymbol{\epsilon} = \sqrt{\bar{\alpha}_t} \mathbf{x}_0 + \sqrt{1 - \bar{\alpha}_t} \boldsymbol{\epsilon}, \quad (10)$$

where  $\alpha_t = 1 - \beta_t$ ,  $\bar{\alpha}_t = \prod_{s=1}^t \alpha_s$ , and  $\boldsymbol{\epsilon} \sim \mathcal{N}(\mathbf{0}, \mathbf{I})$  denotes Gaussian noise. The conditional distribution of  $\mathbf{x}_t$  given  $\mathbf{x}_0$  is

$$q(\mathbf{x}_t | \mathbf{x}_0) \sim \mathcal{N}(\mathbf{x}_t; \sqrt{\bar{\alpha}_t} \mathbf{x}_0, (1 - \bar{\alpha}_t) \mathbf{I}). \quad (11)$$

The proposed method aims to learn the distribution of  $\mathbf{x}_0$  for effective denoising. This can be achieved by optimizing the variational bound on negative log-likelihood, given by [6]

$$\begin{aligned} \mathbb{E}[-\log p_\theta(\mathbf{x}_0)] &\leq \mathbb{E}_q \left[ -\log \frac{p_\theta(\mathbf{x}_{0:T})}{q(\mathbf{x}_{1:T} | \mathbf{x}_0)} \right] \\ &= \mathbb{E}_q \left[ \underbrace{D_{\text{KL}}(q(\mathbf{x}_T | \mathbf{x}_0) \parallel p(\mathbf{x}_T))}_{L_T} - \underbrace{\log p_\theta(\mathbf{x}_0 | \mathbf{x}_1)}_{L_0} \right] \\ &\quad + \sum_{t>1} \underbrace{D_{\text{KL}}(q(\mathbf{x}_{t-1} | \mathbf{x}_t, \mathbf{x}_0) \parallel p_\theta(\mathbf{x}_{t-1} | \mathbf{x}_t))}_{L_{t-1}}, \end{aligned} \quad (12)$$

where  $D_{\text{KL}}(\cdot)$  denotes the Kullback-Leibler (KL) divergence. The third term measures the mismatch between the true distribution and the parameterized distribution and is optimized to ensure that the parameterized distribution closely approximates the true one.  $q(\mathbf{x}_{t-1} | \mathbf{x}_t, \mathbf{x}_0)$  can be derived via Bayes' rule as

$$q(\mathbf{x}_{t-1} | \mathbf{x}_t, \mathbf{x}_0) = \frac{q(\mathbf{x}_t | \mathbf{x}_{t-1}, \mathbf{x}_0) q(\mathbf{x}_{t-1} | \mathbf{x}_0)}{q(\mathbf{x}_t | \mathbf{x}_0)}. \quad (13)$$

Combining (11) and (13), we derive

$$\begin{aligned} q(\mathbf{x}_{t-1} | \mathbf{x}_t, \mathbf{x}_0) \\ \sim \mathcal{N} \left( \frac{\sqrt{\bar{\alpha}_{t-1}} \beta_t}{1 - \bar{\alpha}_t} \mathbf{x}_0 + \frac{\sqrt{\bar{\alpha}_t} (1 - \bar{\alpha}_{t-1})}{1 - \bar{\alpha}_t} \mathbf{x}_t, \frac{1 - \bar{\alpha}_{t-1}}{1 - \bar{\alpha}_t} \beta_t \mathbf{I} \right). \end{aligned} \quad (14)$$

With a specific parameterization of  $p_\theta(\mathbf{x}_{t-1} | \mathbf{x}_t)$ , defined as

$$\begin{aligned} p_\theta(\mathbf{x}_{t-1} | \mathbf{x}_t) \\ \sim \mathcal{N} \left( \mathbf{x}_{t-1}; \frac{1}{\sqrt{\bar{\alpha}_t}} \left( \mathbf{x}_t - \frac{\beta_t}{\sqrt{1 - \bar{\alpha}_t}} \boldsymbol{\epsilon}_\theta(\mathbf{x}_t, t) \right), \sigma_t^2 \mathbf{I} \right), \end{aligned} \quad (15)$$

$L_{t-1}$  can be calculated in a Rao-Blackwellized fashion with closed-form expressions [6]. To summarize, the neural network's loss function can be formulated as

$$L(\theta) = \mathbb{E}_{\mathbf{x}_0, \boldsymbol{\epsilon}, t} [\|\boldsymbol{\epsilon} - \boldsymbol{\epsilon}_\theta(\mathbf{x}_t, t)\|^2]. \quad (16)$$

---

#### Algorithm 1 Training Algorithm

---

**Input:** Training set  $\mathcal{X}$ , hyper-parameter  $T$  and  $\{\beta_t\}_{t=1}^T$

**Output:** Trained model  $\boldsymbol{\epsilon}_\theta(\mathbf{x}_t, t)$

- 1: **repeat**
  - 2:   Sample  $\mathbf{X}$  from  $\mathcal{X}$ ;
  - 3:   Sample  $t$  uniformly from  $\{1, \dots, T\}$ ;
  - 4:   Compute  $\mathbf{X}_t$  based on (10);
  - 5:   Take gradient descent step according to (16);
  - 6: **until** converged
- 

---

#### Algorithm 2 Sampling Algorithm

---

**Input:** Received signal  $\mathbf{Y}$ , starting step index  $t_s$

**Output:**  $\hat{\mathbf{H}}$

- 1:  $\mathbf{X}_{t_s} = \text{fft}(\frac{1}{\sqrt{1+\sigma^2}} \mathbf{Y})$ ;
  - 2: **for**  $m = t_s, \dots, 2$  **do**
  - 3:   Compute  $\mathbf{X}_{m-1}$  according to (18);
  - 4: **end for**
  - 5:  $t = 1$ ;
  - 6:  $\mathbf{X}_0 = \frac{1}{\sqrt{\bar{\alpha}_1}} (\mathbf{X}_1 - \sqrt{1 - \bar{\alpha}_1} \boldsymbol{\epsilon}_\theta(\mathbf{X}_1, 1))$ ;
  - 7:  $\hat{\mathbf{H}} = \text{ifft}(\mathbf{X}_0) \mathbf{P}^\dagger$ ;
- 

Through the training process, the proposed method is capable of estimating the noise in  $\mathbf{x}_t$ , as  $p_\theta(\mathbf{x}_{t-1} | \mathbf{x}_t)$  is optimized to approximate  $q(\mathbf{x}_{t-1} | \mathbf{x}_t, \mathbf{x}_0)$ . To facilitate training, we adopt the angular domain representation as in [11]. Accordingly, the training dataset is constructed as  $\mathcal{X} = \{\mathbf{X}_n = \text{fft}(\mathbf{H}_n \mathbf{P})\}_{n=1}^{N_{\text{train}}}$ , where  $\text{fft}(\cdot)$  denotes the two-dimensional (2D) fast Fourier transform (FFT). In summary, the training algorithm is outlined in Algorithm 1<sup>1</sup>.

#### B. Sampling Algorithm of the Proposed Method

Based on the trained network  $\boldsymbol{\epsilon}_\theta$ , an estimate of  $\mathbf{x}_0$  can be obtained by replacing  $\boldsymbol{\epsilon}$  with  $\boldsymbol{\epsilon}_\theta$  in (10), as follows

$$\hat{\mathbf{x}}_0 = \frac{1}{\sqrt{\bar{\alpha}_t}} (\mathbf{x}_t - \sqrt{1 - \bar{\alpha}_t} \boldsymbol{\epsilon}_\theta(\mathbf{x}_t, t)). \quad (17)$$

According to [16],  $q(\mathbf{x}_{t-1} | \mathbf{x}_t, \mathbf{x}_0)$  can be estimated from  $p_\theta(\mathbf{x}_{t-1} | \mathbf{x}_t, \hat{\mathbf{x}}_0)$ . Therefore, the sampling process is given by

$$\begin{aligned} \mathbf{x}_{t-1} &= \underbrace{\sqrt{\bar{\alpha}_{t-1}} \left( \frac{\mathbf{x}_t - \sqrt{1 - \bar{\alpha}_t} \boldsymbol{\epsilon}_\theta(\mathbf{x}_t, t)}{\sqrt{\bar{\alpha}_t}} \right)}_{\text{estimate } \mathbf{x}_0} \\ &\quad + \underbrace{\sqrt{1 - \bar{\alpha}_{t-1}} \boldsymbol{\epsilon}_\theta(\mathbf{x}_t, t)}_{\text{direction pointing to } \mathbf{x}_t}. \end{aligned} \quad (18)$$

Given (9) and (10), when  $\sqrt{\bar{\alpha}_{t_s}} = \frac{1}{\sqrt{1+\sigma^2}}$ , the KL divergence is  $D_{\text{KL}}(q(\mathbf{x}_{t_s} | \mathbf{x}_0) \parallel p(\mathbf{y} | \mathbf{x}_0)) = 0$ . This indicates that the forward process yields signals that share the same distribution as the received signals. Here,  $\mathbf{x}_{t_s}$  denotes the signal at step  $t_s$  in the forward process. Therefore, during the sampling process, we can start from an intermediate step  $t_s$  rather than from step  $T$  as done in [6], which significantly improves the efficiency. The index  $t_s$  is computed as

<sup>1</sup>Consistent with [6] and [11], the vectorized form is employed for theoretical analysis, whereas the matrix form is used in practical implementations.

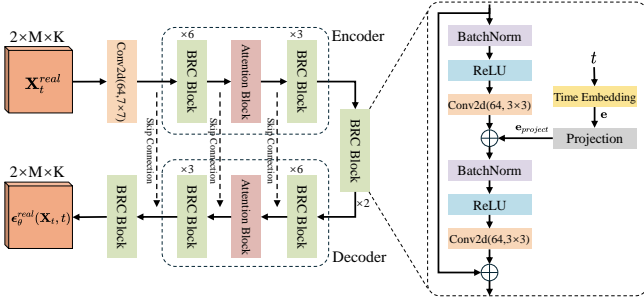


Fig. 2. The architecture of the proposed network.

$$t_s = \arg \min_t \left| 2\sigma^2 - \frac{1 - \bar{\alpha}_t}{\bar{\alpha}_t} \right|, \quad (19)$$

which is referred to as the step-matching mechanism. The starting step depends on the noise level, with larger indices indicating stronger noise contamination and thus requiring more denoising steps. By incorporating (19), the proposed approach can adapt to varying noise conditions without retraining.

In summary, the sampling process starts from the received signal, determines the starting step index according to (19), and repeatedly applies (18) to obtain the denoised original signal  $\mathbf{X}_0$ . The channel estimation result  $\hat{\mathbf{H}}$  is then obtained by applying the inverse fast Fourier transform, denoted as  $\text{ifft}(\cdot)$ , to the denoised signal  $\mathbf{X}_0$ , and subsequently multiplying the result by the pseudo-inverse of  $\mathbf{P}$ , denoted as  $\mathbf{P}^\dagger$ . The proposed sampling algorithm is outlined in Algorithm 2.

### C. Network Architecture Design

In this subsection, we present a detailed description of the proposed BRCNet architecture, as illustrated in Fig. 2.

1) *Preprocess*: To facilitate network processing, the complex-valued matrix  $\mathbf{X}_t \in \mathbb{C}^{M \times K}$  is first decomposed into its real part  $\Re(\mathbf{X}_t)$  and imaginary part  $\Im(\mathbf{X}_t)$ , and then rearranged into a three-dimension (3D) tensor  $\mathbf{X}_t^{real} \in \mathbb{R}^{2 \times M \times K}$ .

2) *Conv2d(64, 7x7)*: Convolutional layers have been widely adopted in image processing tasks due to their ability to capture local correlations between pixels. Since both channel matrices and images can be represented in matrix form, we apply a convolutional layer with 64 output channels and a 7x7 kernel, denoted as  $\text{Conv2d}(64, 7 \times 7)$ , to effectively extract correlations among elements within the input.

3) *Encoder*: Motivated by the architectural efficiency and denoising effectiveness of DnCNN [17], we adapt its design principles to channel estimation and introduce a novel BRC block. Specifically, this block consists of **B**atch normalization (BN) layers, **R**eLU activation functions, and **C**onvolutional layers to extract multi-level features efficiently. To further enhance the model's capability, we integrate the self-attention mechanism. This tailored design not only improves denoising performance but also reduces model complexity, making it well-suited for practical wireless communication scenarios.

Temporal information  $t$  is embedded into each BRC block via a sinusoidal positional embedding vector  $\mathbf{e} \in \mathbb{R}^{N_{embed}}$ , enabling the model to capture temporal dependencies. The

embedding vector is then projected into  $\mathbf{e}_{project} \in \mathbb{R}^{N_{project}}$  to facilitate subsequent computations by a projection module consisting of a Swish activation function and a linear layer.

4) *Decoder*: The decoder adopts a structure similar to that of the encoder. To further extract hierarchical features, skip connections are employed to fuse multi-level information by concatenating feature maps from corresponding layers.

5) *Postprocess*: The model outputs the estimated noise  $\epsilon_\theta^{real}(\mathbf{X}_t, t) \in \mathbb{R}^{2 \times M \times K}$ , which is subsequently transformed into a complex-valued matrix  $\epsilon_\theta(\mathbf{X}_t, t) \in \mathbb{C}^{M \times K}$  by reversing the preprocessing steps applied to the model input.

## IV. NUMERICAL RESULTS

### A. Experiment Setup

We evaluate the proposed method under four scenarios, combining two carrier frequencies ( $f_c = 28$  GHz and  $f_c = 73$  GHz) with two propagation environments: Indoor Hotspot (InH) and Urban Microcell (UMi). The normalized mean square error (NMSE), defined as  $\text{NMSE} = \mathbb{E}[\|\hat{\mathbf{H}} - \mathbf{H}\|_F^2 / \|\mathbf{H}\|_F^2]$ , is adopted as the evaluation metric. The 3D coordinates  $(x, y, z)$  of the UE, BS, and RIS (in meters) are set to  $(0, 25, 2)$ ,  $(38, 48, 1)$ , and  $(40, 50, 2)$  for InH, and  $(0, 25, 20)$ ,  $(80, 75, 1)$ , and  $(70, 85, 10)$  for UMi.

For the channel configuration, the parameters are set as follows:  $M = M_h \times M_v = 8 \times 8$ ,  $N = N_h \times N_v = 4 \times 4$ , and  $K = 17$ . According to [18], the number of clusters follows a Poisson distribution, i.e.,  $C \sim \max\{\mathcal{P}(\lambda_p), 1\}$ , where  $\lambda_p$  is set to 1.8 for  $f_c = 28$  GHz, and to 1.9 for  $f_c = 73$  GHz. The number of scatterers within each cluster follows a uniform distribution:  $S_c \sim \mathcal{U}[1, 30]$ .  $\zeta$  is set to 0.285, and the angular spread is configured as  $\sigma_\varphi = \sigma_\phi = 5^\circ$ . The environment-specific parameters used in (3) are configured as: InH(LOS):  $n = 1.73$ ,  $\sigma_x = 3.02$  dB,  $b = 0$ ; InH(NLOS):  $n = 3.19$ ,  $\sigma_x = 8.29$  dB,  $b = 0.06$ ; UMi(LOS):  $n = 1.98$ ,  $\sigma_x = 3.1$  dB,  $b = 0$ ; UMi(NLOS):  $n = 3.19$ ,  $\sigma_x = 8.2$  dB,  $b = 0$ . The carrier frequency for all cases is  $f_0 = 24.2$  GHz. Notably, for the InH scenario, the RIS is assumed to be sufficiently close to the BS such that the RIS-BS channel comprises only the LOS component, further highlighting the distinct characteristics between different scenarios. For the proposed method, the hyperparameters are set as follows:  $T = 1000$ , the variance schedule  $\{\beta_t\}$  increases linearly from  $\beta_0 = 1 \times 10^{-4}$  to  $\beta_T = 0.02$ . The training set consists of 50,000 samples, while the validation and test sets contain 10,000 samples each.

### B. Results and Analysis

In the simulations, the proposed method is compared against the following baselines: (i) the classical least squares (LS) algorithm; (ii) the linear minimum mean square error (LMMSE) algorithm; (iii) DS\_OMP [3], the double-structured orthogonal matching pursuit algorithm; (iv) CDRN [4], which employs a deep convolutional network to denoise LS estimation results; (v) DM-CNN1 [11], a method based on denoising diffusion probabilistic models (DDPMs) with a CNN-based network; and (vi) DM-CNN2, an enhanced version of DM-CNN1 with an increased number of convolutional layers and feature channels to ensure a fair comparison. For the proposed method,

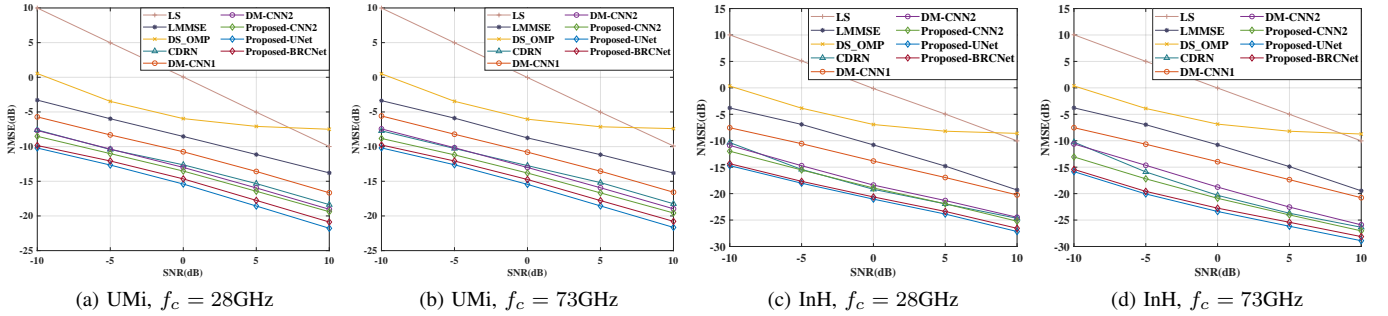


Fig. 3. NMSE performance versus SNR under different scenarios:(a) UMi,  $f_c = 28\text{GHz}$ . (b) UMi,  $f_c = 73\text{GHz}$ . (c) InH,  $f_c = 28\text{GHz}$ . (d) InH,  $f_c = 73\text{GHz}$ .

TABLE I  
PARAMETERS AND COMPLEXITY COMPARISON

Model	Parameters	MACs
CNN1	55.03K	57.32M
CNN2	2.38M	2.58G
U-Net	25.81M	7.97G
Proposed BRCNet	2.41M	2.18G

we implement three different network architectures: CNN2, U-Net, and the proposed BRCNet.

Fig. 3 illustrates the NMSE performance of different methods under varying SNR conditions. Specifically, in Fig. 3(a) at 0 dB, the proposed BRCNet-based method achieves performance gains of 14.70 dB, 6.12 dB, 8.69 dB, 2.03 dB, 3.91 dB, 1.65 dB, and 1.13 dB over LS, LMMSE, DS\_OMP, CDRN, DM-CNN1, DM-CNN2, and Proposed-CNN2, respectively. Unlike CDRN’s direct-mapping method, the proposed method achieves improved performance through progressive denoising. Compared with DM-CNN1 and DM-CNN2, simulation results show that the proposed method is more effective. Moreover, the proposed BRCNet achieves performance highly comparable to U-Net, with the performance gap within 0.91 dB, while significantly reducing the number of parameters.

Table I compares the number of parameters and the number of multiply-accumulate operations (MACs) of DM-based methods. Although CNN1 has fewer parameters, its limited model capacity leads to poor performance in complex channel environments. In contrast, CNN2 has a similar parameter count to the BRCNet but still underperforms in terms of NMSE, highlighting the effectiveness of the proposed network architecture. Notably, BRCNet achieves performance comparable to U-Net with only 9.34% of its parameters, offering an excellent trade-off among model complexity, computational overhead, and estimation accuracy. Moreover, compared with CDRN, the proposed method can adapt to different SNRs without retraining, further reducing storage requirements and computational overhead in practical applications.

## V. CONCLUSION

In this letter, we propose a DM-aided channel estimation method by formulating the estimation task as the reverse process of DMs, which adapts to varying noise levels. To reduce model complexity, we further design a parameter-efficient network, BRCNet, which achieves comparable performance with

substantially fewer parameters. Simulation results demonstrate that the proposed method significantly outperforms baselines.

## REFERENCES

- [1] C.-X. Wang *et al.*, “On the road to 6g: Visions, requirements, key technologies, and testbeds,” *IEEE Commun. Surveys Tuts.*, vol. 25, no. 2, pp. 905–974, 2023.
- [2] Q. Wu and R. Zhang, “Towards smart and reconfigurable environment: Intelligent reflecting surface aided wireless network,” *IEEE Commun. Mag.*, vol. 58, no. 1, pp. 106–112, 2019.
- [3] X. Wei, D. Shen, and L. Dai, “Channel estimation for ris assisted wireless communications—part ii: An improved solution based on double-structured sparsity,” *IEEE Commun. Lett.*, vol. 25, no. 5, pp. 1403–1407, 2021.
- [4] C. Liu *et al.*, “Deep residual learning for channel estimation in intelligent reflecting surface-assisted multi-user communications,” *IEEE Trans. Wireless Commun.*, vol. 21, no. 2, pp. 898–912, 2021.
- [5] H. Feng and Y. Zhao, “mmWave RIS-assisted SIMO channel estimation based on global attention residual network,” *IEEE Wireless Commun. Lett.*, vol. 12, no. 7, pp. 1179–1183, 2023.
- [6] J. Ho, A. Jain, and P. Abbeel, “Denoising diffusion probabilistic models,” in *Proc. Neural Inf. Process. Syst.*, vol. 33, 2020, pp. 6840–6851.
- [7] T. Wu *et al.*, “CDDM: Channel denoising diffusion models for wireless semantic communications,” *IEEE Trans. Wireless Commun.*, vol. 23, no. 9, pp. 11 168–11 183, 2024.
- [8] X. Guan *et al.*, “Joint design of denoising diffusion probabilistic models and ldpc decoding for wireless communications,” in *2024 IEEE Int. Conf. Commun. (ICC Workshops)*, 2024, pp. 1944–1949.
- [9] X. Zhou *et al.*, “Generative diffusion models for high dimensional channel estimation,” *IEEE Trans. Wireless Commun.*, pp. 1–1, 2025.
- [10] W. Tong *et al.*, “Diffusion model-based channel estimation for RIS-aided communication systems,” *IEEE Wireless Commun. Lett.*, 2024.
- [11] B. Fesl *et al.*, “Diffusion-based generative prior for low-complexity MIMO channel estimation,” *IEEE Wireless Commun. Lett.*, 2024.
- [12] 3GPP, “Study on channel model for frequencies from 0.5 to 100 GHz,” 3GPP, Technical Report TR 38.901, 2018. [Online]. Available: [https://www.3gpp.org/ftp/Specs/archive/38\\_series/38.901/](https://www.3gpp.org/ftp/Specs/archive/38_series/38.901/)
- [13] E. Basar, I. Yildirim, and F. Kilinc, “Indoor and outdoor physical channel modeling and efficient positioning for reconfigurable intelligent surfaces in mmwave bands,” *IEEE Trans. Commun.*, vol. 69, no. 12, pp. 8600–8611, 2021.
- [14] P. Nayeri, F. Yang, and A. Z. Elsherbeni, *Reflectarray antennas: theory, designs, and applications*. USA: Wiley, 2018.
- [15] B. Zheng and R. Zhang, “Intelligent reflecting surface-enhanced ofdm: Channel estimation and reflection optimization,” *IEEE Wireless Commun. Lett.*, vol. 9, no. 4, pp. 518–522, 2020.
- [16] J. Song, C. Meng, and S. Ermon, “Denoising diffusion implicit models,” in *Proc. Int. Conf. Learn. Represent.*, 2021, pp. 1–22.
- [17] K. Zhang *et al.*, “Beyond a gaussian denoiser: Residual learning of deep cnn for image denoising,” *IEEE Trans. Image Process.*, vol. 26, no. 7, pp. 3142–3155, 2017.
- [18] I. A. Hemadeh *et al.*, “Millimeter-wave communications: Physical channel models, design considerations, antenna constructions, and link-budget,” *IEEE Commun. Surveys Tuts.*, vol. 20, no. 2, pp. 870–913, 2018.